Hexamodal Imaging with Porphyrin-Phospholipid-Coated Upconversion Nanoparticles

James Rieffel, Feng Chen, Jeesu Kim, Guanying Chen, Wei Shao, Shuai Shao, Upendra Chitgupi, Reinier Hernandez, Stephen A. Graves, Robert J. Nickles, Paras N. Prasad,* Chulhong Kim, Weibo Cai, and Jonathan F. Lovell**

Biomedical imaging has become a cornerstone of modern medicine.[1] Progress in imaging technologies stimulates development of novel and facultative contrast agents, reinforcing cyclical patterns of innovation. With clinical implementation of combined positron emission tomography/ X-ray computed tomography (PET/CT) and PET/MR (magnetic resonance) scanners, there has been an increasing interest in integrated imaging systems that yield information not accessible by just a single modality. Concurrently, there have been numerous recent reports of contrast agents that enable not only mostly bi-, but also tri- and tetra-modal medical imaging capabilities.[2]

Some representative examples include functionalized gold for CT/MR/ultrasound[3] and photoacoustic (PA)/MR/Raman;[4] functionalized iron oxide for fluorescence (FL)/MR/PET,[5] FL/MR/CT,[6] and FL/MR/PET/Bioluminescence;[7] polymeric porphyrins for FL/MR/PET;[8] melanin nanoparticles for PA/MR/PET;[9] liposomes for FL/Cerenkov luminescence (CL)/MR;[10] and upconversion nanoparticles (UCNPs) for UC/MR/CT,[11] upconversion (UC)/MR/CT/SPECT,[12] and higher order theranostic paradigms.[13] Here, a simple approach is proposed in which a nanoparticulate agent, readily formed from just two active components, can be used to explore imaging parameters in six modalities.

The multimodal nanoparticle is a porphyrin-phospholipid (PoP)-coated UCNP (**Figure 1**a). We recently demonstrated that PoP can be synthesized and used to form theranostic nanovesicles, as well as be used to coat other nanoparticles.[14] The PoP coating directly confers near-infrared (NIR) biophotonic properties of conventional FL and PA to the UCNP. Additionally, based on the exquisite affinity of copper for porphyrins, the nanoparticles can be seamlessly postlabeled for PET and CL imaging by simple incubation with ^{64}Cu.[15] The UCNP (core-shell of $NaYbF_4$:Tm-$NaYF_4$) used was rationally designed for NIR-to-NIR UC luminescence imaging, and the dense electron content is also suitable for detection in CT. Due to their versatility and propensity for deep and low-background optical imaging, UCNPs have attracted considerable interest recently.[16]

PoP-UCNPs were generated by coating oleic acid-capped UCNPs, synthesized via thermal decomposition,[17] with phospholipids to render them dispersible in aqueous solutions. Thin films containing PoP-UCNPs with varying ratios of PoP to

J. Rieffel, S. Shao, U. Chitgupi, Prof. J. F. Lovell
Department of Biomedical Engineering
University at Buffalo
State University of New York
Buffalo, NY 14260, USA
E-mail: jflovell@buffalo.edu
Dr. F. Chen, R. Hernandez, S. A. Graves, Prof. R. J. Nickles, Prof. W. Cai
Department of Radiology and Medical Physics
University of Wisconsin
Madison, WI 53705, USA
J. Kim, Prof. C. Kim
Department of Creative IT Engineering and Department of Electrical Engineering
POSTECH
Pohang, Korea
Prof. G. Chen, W. Shao
School of Chemical Engineering and Technology
Harbin Institute of Technology
Harbin, P.R. China
E-mail: chenguanying@hit.edu.cn
Prof. G. Chen, W. Shao, Prof. P. N. Prasad
Institute for Lasers Photonics and Biophotonics
Department of Chemistry
University at Buffalo
State University of New York
Buffalo, NY 14260, USA
E-mail: pnprasad@buffalo.edu

DOI: 10.1002/adma.201404739

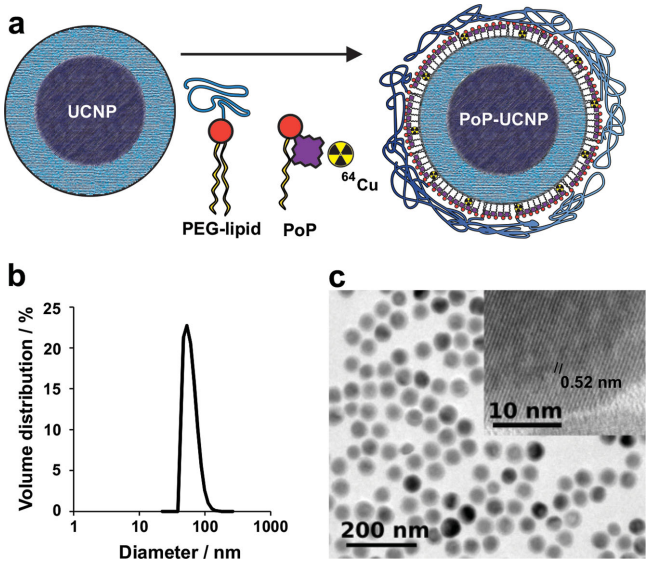

Figure 1. PoP-UCNPs. a) Schematic diagram of the PoP-UCNP structure. Core-shell UCNPs were transferred to the aqueous phase by lipid coating with PEG-lipid and PoP. Radioactive ^{64}Cu can seamlessly chelate inside PoP. b) Size distribution of PoP-UCNPs as determined by dynamic light scattering. c) Electron micrographs of PoP-UCNPs. High-magnification inset demonstrates the characteristic crystalline structure and the UCNP core/shell geometry.

polyethylene glycol (PEG)-lipid were hydrated with water and sonicated to generate stable and dispersed nanoparticles. Transmission electron microscopy and dynamic light scattering of PoP-UCNPs coated with 80 molar% PoP and 20 molar% PEG-lipid revealed an average particle size of 74 nm (standard deviation of 3.6 nm for triplicate measurements) and a polydispersity index of 0.12 (Figure 1b,c), indicating minimal aggregation occurred after the surface modification. Electron micrographs, which were taken without negative staining and thus would not detect the PEG coating, revealed a diameter close to 60 nm. At higher resolution, micrographs revealed a crystal lattice spacing of 0.52 nm, which is close to the 0.51 nm spacing expected for a crystal plane of hexagonal $NaYbF_4$ with a Miller index of 100.[18] Additional electron micrographs clearly depicting the core-shell structure of the UCNP and an energy dispersive X-ray spectrum confirming the chemical composition are found in Figures S1 and S2 (Supporting Information). The NIR emission of the UCNPs close to 800 nm following 980 nm excitation is from the $^3H_4 \rightarrow {}^3H_6$ transition of the Tm^{3+}. The dependence of this emission intensity on excitation power was investigated and indicated that the generation of UC emission involved a two-photon process (Figure S3, Supporting Information), in agreement with our previous observations on UC photophysics.[19]

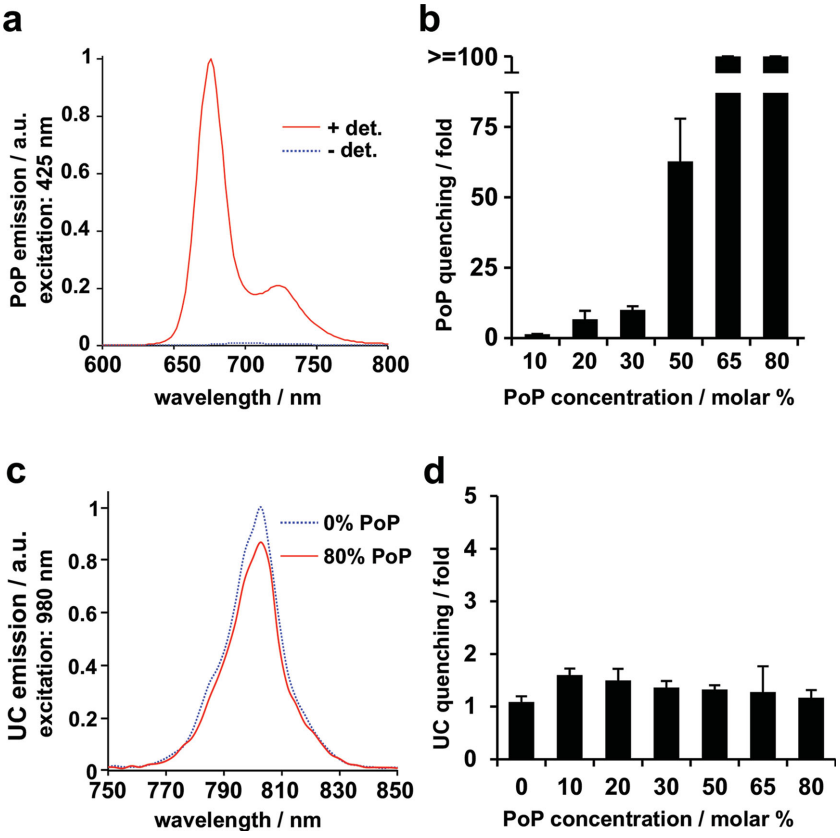

Figure 2. Optical emission properties of PoP-UCNPs. a) PoP FL self-quenching of intact (–detergent) compared to dissociated (+detergent) PoP-UCNPs (coating comprising 80 molar% PoP, 20 molar% PEG-lipid). b) PoP self-quenching as a function of the molar% PoP incorporated into the UCNP coating. Values were calculated by comparing +det. and –det. samples. c) UC spectra of PoP-UCNPs (80 mol.% PoP, 20 mol.% PEG-lipid) compared to UCNPs coated with the PEG-lipid alone. 980 nm excitation was used. d) UC quenching as a function of molar% PoP incorporated into the UCNP coating. The values close to unity indicate an absence of UC quenching.

Based on their dense self-packing in a spatially constrained bilayer, PoP bilayers give rise to intense intermolecular porphyrin face-to-face contact and FL self-quenching. PoP FL can be restored by addition of detergent, which destroys the bilayer structure as well as self-quenching effects resulting from extreme porphyrin density. In order to study the self-quenching of PoP-UCNPs, varied molar percentages ranging from 0% to 80% PoP were used to coat the particles during the surface modification process. The self-quenching of PoP FL was tested by comparing PoP-UCNPs with and without addition of detergent (+det. and -det.). The FL spectrum of PoP-UCNPs containing 80% molar PoP (**Figure 2**a) shows that without detergent, the emission peak at 675 nm (originating from the PoP itself) was virtually completely quenched. With the addition of detergent, a greater than 100-fold increase in signal was observed. Figure 2b further shows the degree of PoP self-quenching for various molar ratios. As more PoP is titrated into the bilayer coating, interPoP reactions and face-to-face porphyrin stacking becomes more pronounced, leading to extreme self-quenching. This self-quenching phenomenon enables convenient monitoring of the stability of the PoP coating and therefore, the PoP-UCNP itself. This may also enable convenient monitoring of PoP-UCNP stability in blood or cellular uptake, which also triggers dissociation of the PoP coating.[14b] When incubated in vitro for 24 h at 37 °C, the nanoparticles remained fully intact in phosphate buffered saline and over 75% intact in cell growth medium containing 10% fetal bovine serum (Figure S4, Supporting Information).

The NIR-to-NIR UC process occurs in the deep NIR range, which enables greater tissue penetration depth and thus is a useful optical window for in vivo optical imaging. Therefore, the effects of the PoP coating on the UC of the UCNPs were examined. The UC emission of UCNPs coated with either 80 or 0 molar% PoP (Figure 2c,d) shows that even with the highest PoP concentration in the bilayer, the NIR emission peak at 800 nm remained relatively unquenched. Thus, the PoP coating did not interfere with the photophysics of the UC process. These data indicate that the PoP coating can be applied to UCNPs without losing the most desirable UC luminescence properties. PoP-UCNPs with 80 molar% PoP were used for subsequent in vitro and in vivo multimodality imaging. Twenty percent PEG-lipid was retained in the bilayer since PEG is known to improve nanoparticle steric stability and biocompatibility.[20] When incubated with mammalian cells in vitro for 24 h at 37 °C, PoP-UCNPs did not induce any discernable toxicity up to 1 mg mL^{-1}, which was the highest concentration assessed (Figure S5, Supporting Information).

Adv. Mater. **2015**,
DOI: 10.1002/adma.201404739

PoP nanovesicles and other tetrapyrrolic nanoparticles effectively chelate ^{64}Cu radioisotopes and readily do so in aqueous solution after the nanoparticles have already been formed.[15,21] Postlabeling PoP-UCNPs with ^{64}Cu confers CL and PET imaging capacity. CL involves light emission during the decay of radionuclides and is similar to UC imaging in that conventional autofluorescence interference is greatly diminished. Successful ^{64}Cu labeling was achieved by simply incubating $^{64}CuCl_2$ with PoP-UCNPs in 0.1 M sodium acetate (pH 5.5) at 37 °C for 60 min with shaking. ^{64}Cu-PoP-UCNPs were further purified by gel filtration, eliminating any residual free ^{64}Cu. A representative elution profile shown in Figure S6 (Supporting Information) demonstrates that prior to purification, the ^{64}Cu labeling yield was greater than 80%.

In vitro studies were performed to compare imaging properties between the six different imaging modalities. Imaging was performed with commercial systems with the exception of a custom-built PA system,[22] and PET reconstruction was performed as previously described.[23] Three small diameter tubes were filled with PoP-UCNPs without detergent (–det.), PoP-UCNPs with detergent (+det.), and water (as a control), and imaged in each modality (**Figure 3**a). The nanoparticle concentration was 0.7 mg mL^{-1} in all cases except for the in vitro CT phantom imaging, which used a concentration of 34 mg mL^{-1}. The water tubing control was generally undetectable in all modalities, with the exception of a slight background signal in CT. The samples +det. and -det. generally yielded the same signal intensity, with the exception of FL and PA. In accord with the data shown in Figure 2, when intact (–det.), the PoP-UCNPs yielded a significantly diminished FL signal compared to +det. Conversely, the -det. sample exhibited an enhanced PA signal compared to +det, although the magnitude of the difference was not as pronounced. This phenomenon is not unexpected since FL quenching leads to thermal dissipation of absorbed light energy (as opposed to photon emission), which is directly responsible for generation of the PA signal. Therefore, FL and PA modalities provide indication of the self-assembly status of the PoP-UCNP. This clearly demonstrates how different modalities can yield different information about contrast agents, in this case about the integrity of the particle coating.

PoP-UCNPs were then imaged in a turkey breast phantom to determine depth-dependent signal attenuation and resolution in tissue. Turkey breast tissue was selected to mimic the properties of human breast tissue, since lymph node mapping is a current clinical challenge for determining the metastatic state of breast cancer.[24] For signal attenuation studies, tubing containing PoP-UCNPs was visualized with constant exposure times in each modality under increasing thickness of turkey breast tissue (Figure 3b). The signal, which was scattered or absorbed as it passed through the tissue, was collected in a region of interest over the known location of samples and normalized to the signal

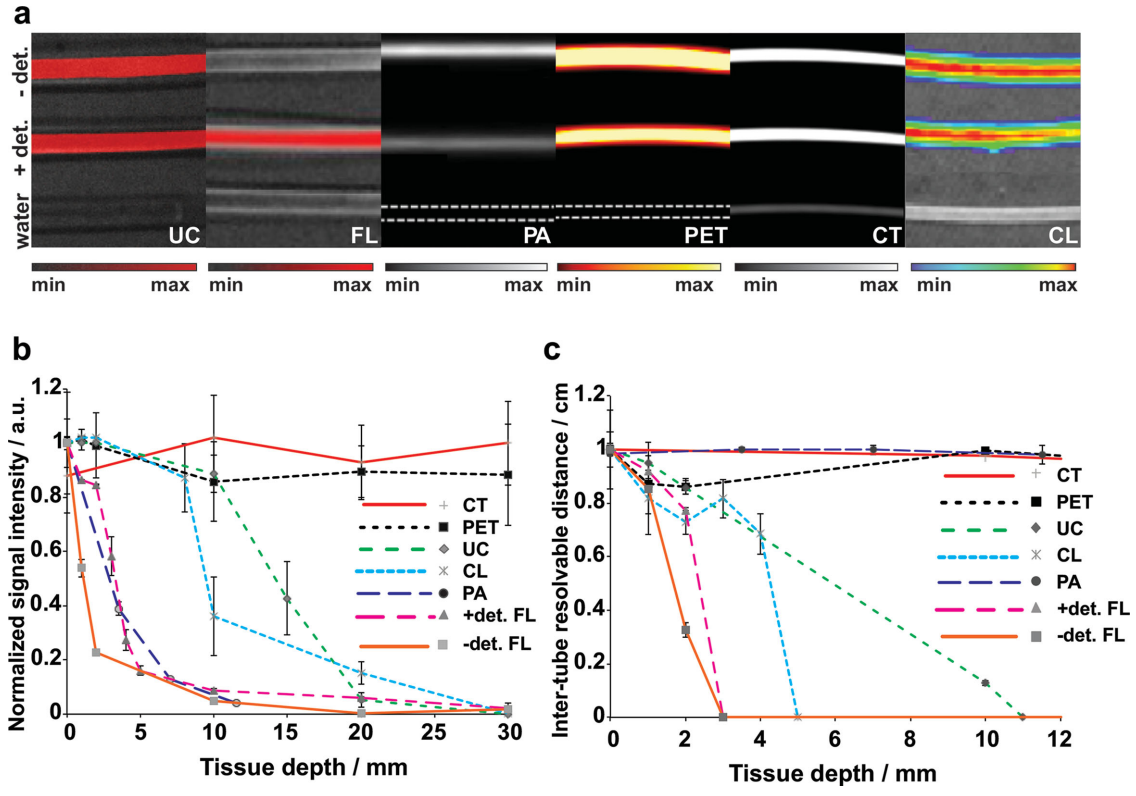

Figure 3. Hexamodal imaging of PoP-UCNPs in vitro. a) Images of PoP-UCNPs in polyethylene tubing (0.86 mm inner diameter). The top tubes contain a solution of intact PoP-UCNPs in water, the middle tubes containing PoP-UCNPs that have been dissociated with detergent and the bottom tubes contain water as a control. b) Signal intensity from phantom samples as a function of tissue depth. Images of an individual phantom sample were obtained for CT, PET, UC, CL, PA, and ±det FL through turkey breast tissue depths ranging from 0 to 30 mm. The signal intensity for each modality was normalized to the signal detected at 0 mm tissue depth (no tissue). c) Identical tubing phantoms were secured 1 cm apart and imaged through increasing depths of turkey breast. The resolvable distance between tubes was then determined.

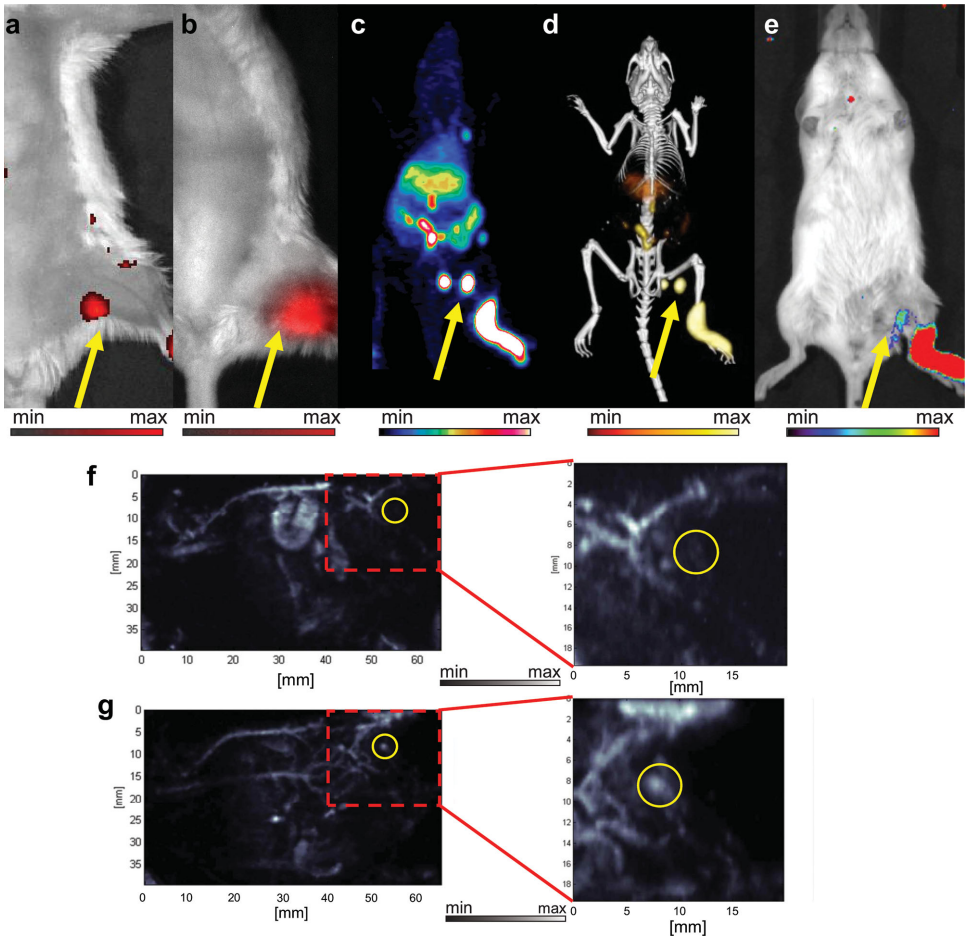

Figure 4. In vivo lymphatic imaging using PoP-UCNPs in mice. PoP-UCNPs were injected in the rear left footpad and imaged in six modalities 1 h post-injection. Accumulation of PoP-UCNPs in the first draining lymph node is indicated with yellow arrows. a) Traditional FL and b) UC images with the injection site cropped out of frame. c) Full anatomy PET, d) merged PET/CT, and e) CL images. f) PA images before and g) after injection show endogenous PA blood signal compared to the contrast enhancement that allowed visualization of the previously undetected lymph node.

obtained without any overlaid tissue. As would be expected for CT and PET, which are whole body clinical imaging techniques, no significant attenuation was seen at the largest tissue depth tested (30 mm). The FL signal of intact PoP-UCNP, which was highly quenched, was attenuated to 50% of the original signal within the first few millimeters of tissue. Disruption of the PoP-UCNP structure with detergent, to increase the PoP FL signal, extended that depth by ≈2 mm. However, it should be noted that for FL with detergent, the imaging signal was saturated for the first couple of mm of tissue. PA signal also attenuated rapidly in tissue, with half the signal being lost before 5 mm. However, it is important to note that the observed signal attenuation for PA and other modalities does not equate to detection sensitivity. Indeed PA signal could be detected under the full 30 mm of tissue. UC and CL exhibited intermediate signal attenuation with the signal becoming half-attenuated between 10 and 15 mm. Because imaging parameters in these modalities can be adjusted to dramatically affect performance metrics like attenuation or sensitivity, and the linearity of the systems was not thoroughly evaluated, these results are meant primarily to demonstrate the multimodal potential of PoP-UCNPs as opposed to representing fully optimized imaging specifications.

Depth-dependent resolution for each modality was then tested by securing two identical samples in tubing exactly 10 mm apart, and again serially imaging under increasing thickness of turkey breast (Figure 3c). The ability to resolve the two samples was plotted as a function of tissue depth and images were processed in ImageJ software by examining the discernable distance between signal peaks. Exposure time in any given modality was maximized to obtain better images prior to analysis. Similarly to the tissue penetration, CT and PET resolved the samples at all depths tested. Interestingly, although the PA signal diminished quickly at larger tissue depths, resolvability was conserved for as long as the signal was clearly separated from the background. This was not the case for UC and FL, for which both lost their signal detectability and resolvability at similar rates, due to the increased rate of optical (as opposed to acoustic in the case of PA) scattering in the tissue.

Due to the clinical importance of lymphatic mapping in oncology, numerous multimodal lymphatic contrast agents have been assessed.[25] PoP-UCNPs were used for in vivo lymphatic imaging (**Figure 4**a–g). Small volume samples (≈20 µL containing 14 µg of PoP-UCNPs for a dose of ≈0.7 mg kg^{-1} body weight) were injected in the left rear footpad

Adv. Mater. **2015**,
DOI: 10.1002/adma.201404739

of BALB/c mice, which were then allowed to move freely. After 1 h, adequate time for lymphatic drainage, the mice were anesthetized and imaged in four different scanners; a PET/CT scanner, a traditional IVIS Spectrum scanner, an IVIS fitted with a 980 nm laser diode source, and custom-made preclinical PA imaging system. The accumulation of PoP-UCNPs in the first draining lymph node was clearly discernable in all systems. In the FL, UC, and CL images, mouse hair was removed to enable better visualization of the individual node, but a large amount of scattering was present even through the thin layer of skin (Figure 4a,b,e). FL and UC images were taken with the footpad injection site masked with tape and out of the image frame. On the contrary, the PET and combined PET/CT imaging revealed not only the sentinel lymph node but also a more extensive lymphatic network (Figure 4c,d). While combined PET/CT imaging provided excellent anatomical registration of PoP-UCNPs in the lymph node, CT by itself was the only modality that could not readily detect the nanoparticles in vivo, suggesting that more optimization is required to generate more CT contrast in the lymph node. Because PA imaging visualizes endogenous chromophores in the blood for signal generation, before and after injection images were taken to illustrate the contrast enhancement (Figure 4f,g). While the PoP-UCNPs were well-tolerated in this study, long-term toxicity studies are required to better assess the safety of the nanoparticles.

In conclusion, PoP-UCNPs are easily formed from only two active imaging components (PoP and UCNPs) yet are active in at least six different imaging modalities. FL, in particular, and PA provided unique information on the self-assembly status of the particles. PET and CT provided the deepest imaging capabilities, although low sensitivity prevented detection of the agent in vivo using CT. CL and UC imaging was effective for less invasive signal detection at intermediate depths substantially deeper than FL. In all cases, the contrast enhancement conferred to these diverse imaging methods shows that engineering simple yet higher-order multimodal imaging agents is feasible and may be useful for the development of hyper-integrated imaging systems.

Supporting Information

Supporting Information is available from the Wiley Online Library or from the author.

Acknowledgements

The authors thank Jumin Geng for assistance with cell and animal studies. This work was supported by research funds from the National Science Foundation (Grant No. DGE-1256259), the National Institutes of Health (Grant Nos. 1R01CA169365, 5T32GM08349, and DP5OD017898), the American Cancer Society (Grant No. 125246-RSG-13–099–01-CCE), the Natural Science Foundation of China (Grant No. 51102066), the Program for the Basic Research Excellent Talents in Harbin Institute of Technology (BRETIII 2012018), the Fundamental Research Funds for the Central Universities (Grant No. HIT. AUGA5710052614) the NIPA IT Consilience Creative Program (Grant No. NIPA-2013-H0203–13–1001), and an NRF Engineering Research Center grant (Grant No. NRF-2011–0030075) of the Ministry of Science, ICT, and Future Planning, Republic of Korea. Animal studies were carried out in accordance with the Institutional Animal Care and Use Committees of POSTECH, University of Wisonsin-Madison and University at Buffalo.

Received: October 13, 2014
Revised: November 28, 2014
Published online:

[1] T. F. Massoud, S. S. Gambhir, *Genes Dev.* **2003**, *17*, 545.
[2] a) S. Lee, X. Chen, *Mol. Imaging* **2009**, *8*, 87; b) D. E. Lee, H. Koo, I. C. Sun, J. H. Ryu, K. Kim, I. C. Kwon, *Chem. Soc. Rev.* **2012**, *41*, 2656; c) A. Louie, *Chem. Rev.* **2010**, *110*, 3146; d) M. Swierczewska, S. Lee, X. Chen, *Mol. Imaging* **2011**, *10*, 3.
[3] D. R. Arifin, C. M. Long, A. A. Gilad, C. Alric, S. Roux, O. Tillement, T. W. Link, A. Arepally, J. W. M. Bulte, *Radiology* **2011**, *260*, 790.
[4] M. F. Kircher, A. de la Zerda, J. V. Jokerst, C. L. Zavaleta, P. J. Kempen, E. Mittra, K. Pitter, R. Huang, C. Campos, F. Habte, R. Sinclair, C. W. Brennan, I. K. Mellinghoff, E. C. Holland, S. S. Gambhir, *Nat. Med.* **2012**, *18*, 829.
[5] M. Yang, K. Cheng, S. B. Qi, H. G. Liu, Y. X. Jiang, H. Jiang, J. B. Li, K. Chen, H. M. Zhang, Z. Cheng, *Biomaterials* **2013**, *34*, 2796.
[6] S. Xue, Y. Wang, M. Wang, L. Zhang, X. Du, H. Gu, C. Zhang, *Int. J. Nanomedicine* **2014**, *9*, 2527.
[7] W. Hwang do, H. Y. Ko, S. K. Kim, D. Kim, D. S. Lee, S. Kim, *Chemistry* **2009**, *15*, 9387.
[8] Y. Li, T. Y. Lin, Y. Luo, Q. Liu, W. Xiao, W. Guo, D. Lac, H. Zhang, C. Feng, S. Wachsmann-Hogiu, J. H. Walton, S. R. Cherry, D. J. Rowland, D. Kukis, C. Pan, K. S. Lam, *Nat. Commun.* **2014**, *5*, 4712.
[9] Q. Fan, K. Cheng, X. Hu, X. Ma, R. Zhang, M. Yang, X. Lu, L. Xing, W. Huang, S. S. Gambhir, Z. Cheng, *J. Am. Chem. Soc.* **2014**, *136*, 15185.
[10] C. Kim, C. Favazza, L. V. Wang, *Chem. Rev.* **2010**, *110*, 2756.
[11] a) J.-W. Shen, C.-X. Yang, L.-X. Dong, H.-R. Sun, K. Gao, X.-P. Yan, *Anal. Chem.* **2013**, *85*, 12166; b) Z. Liu, K. Dong, J. Liu, X. Han, J. Ren, X. Qu, *Small* **2014**, *10*, 2429; c) D. Yang, Y. Dai, J. Liu, Y. Zhou, Y. Chen, C. Li, P. a. Ma, J. Lin, *Biomaterials* **2014**, *35*, 2011; d) D. Ni, W. Bu, S. Zhang, X. Zheng, M. Li, H. Xing, Q. Xiao, Y. Liu, Y. Hua, L. Zhou, W. Peng, K. Zhao, J. Shi, *Adv. Funct. Mater.* **2014**, *24*, 6612. e) X. Zhu, J. Zhou, M. Chen, M. Shi, W. Feng, F. Li, *Biomaterials* **2012**, *33*, 4618; f) Q. Xiao, W. Bu, Q. Ren, S. Zhang, H. Xing, F. Chen, M. Li, X. Zheng, Y. Hua, L. Zhou, W. Peng, H. Qu, Z. Wang, K. Zhao, J. Shi, *Biomaterials* **2012**, *33*, 7530; g) H. Xing, W. Bu, S. Zhang, X. Zheng, M. Li, F. Chen, Q. He, L. Zhou, W. Peng, Y. Hua, J. Shi, *Biomaterials* **2012**, *33*, 1079.
[12] Y. Sun, X. Zhu, J. Peng, F. Li, *ACS Nano* **2013**, *7*, 11290.
[13] a) W. P. Fan, B. Shen, W. B. Bu, F. Chen, Q. J. He, K. L. Zhao, S. J. Zhang, L. P. Zhou, W. J. Peng, Q. F. Xiao, D. L. Ni, J. N. Liu, J. L. Shi, *Biomaterials* **2014**, *35*, 8992; b) J. Shen, L. Zhao, G. Han, *Adv. Drug Delivery Rev.* **2013**, *65*, 744; c) L. Cheng, K. Yang, Y. Li, J. Chen, C. Wang, M. Shao, S.-T. Lee, Z. Liu, *Angew. Chem Int. Ed.* **2011**, *123*, 7523; d) L. Cheng, K. Yang, Y. Li, X. Zeng, M. Shao, S.-T. Lee, Z. Liu, *Biomaterials* **2012**, *33*, 2215.
[14] a) N. C. Tam, P. Z. McVeigh, T. D. MacDonald, A. Farhadi, B. C. Wilson, G. Zheng, *Bioconjugate Chem.* **2012**, *23*, 1726; b) J. F. Lovell, C. S. Jin, E. Huynh, T. D. MacDonald, W. Cao, G. Zheng, *Angew. Chem Int. Ed.* **2012**, *51*, 2429; c) J. F. Lovell, C. S. Jin, E. Huynh, H. Jin, C. Kim, J. L. Rubinstein, W. C. Chan, W. Cao, L. V. Wang, G. Zheng, *Nat. Mater.* **2011**, *10*, 324; d) K. A. Carter, S. Shao, M. I. Hoopes, D. Luo, B. Ahsan, V. M. Grigoryants, W. Song, H. Huang, G. Zhang, R. K. Pandey,

J. Geng, B. A. Pfeifer, C. P. Scholes, J. Ortega, M. Karttunen, J. F. Lovell, *Nat. Commun.* **2014**, *5*, 3546.
[15] T. W. Liu, T. D. MacDonald, J. Shi, B. C. Wilson, G. Zheng, *Angew. Chem Int. Ed.* **2012**, *51*, 13128.
[16] a) J. Zhou, Z. Liu, F. Y. Li, *Chem. Soc. Rev.* **2012**, *41*, 1323; b) X. Wu, G. Chen, J. Shen, Z. Li, Y. Zhang, G. Han, *Bioconjugate Chem.* **2014**, DOI: 10.1021/bc5003967; c) Q. Liu, W. Feng, F. Y. Li, *Coord. Chem. Rev.* **2014**, *273*, 100; d) Y. I. Park, K. T. Lee, Y. D. Suh, T. Hyeon, *Chem. Soc. Rev.* **2014**, DOI: 10.1039/c4cs00173g; e) L. Cheng, C. Wang, Z. Liu, *Nanoscale* **2013**, *5*, 23. f) G. Chen, H. Qiu, P. N. Prasad, X. Chen, *Chem. Rev.* **2014**, *114*, 5161.
[17] J.-C. Boyer, F. Vetrone, L. A. Cuccia, J. A. Capobianco, *J. Am. Chem. Soc.* **2006**, *128*, 7444.
[18] L. Pan, M. He, J. Ma, W. Tang, G. Gao, R. He, H. Su, D. Cui, *Theranostics* **2013**, *3*, 210.
[19] a) G. Chen, J. Shen, T. Y. Ohulchanskyy, N. J. Patel, A. Kutikov, Z. Li, J. Song, R. K. Pandey, H. Ågren, P. N. Prasad, G. Han, *ACS Nano* **2012**, *6*, 8280; b) G. Chen, T. Y. Ohulchanskyy, R. Kumar, H. Ågren, P. N. Prasad, *ACS Nano* **2010**, *4*, 3163.
[20] J. V. Jokerst, T. Lobovkina, R. N. Zare, S. S. Gambhir, *Nanomedicine* **2011**, *6*, 715.
[21] Y. Zhang, M. Jeon, L. J. Rich, H. Hong, J. Geng, Y. Zhang, S. Shi, T. E. Barnhart, P. Alexandridis, J. D. Huizinga, M. Seshadri, W. Cai, C. Kim, J. F. Lovell, *Nat. Nanotechnol.* **2014**, *9*, 631.
[22] M. Jeon, J. Kim, C. Kim, *Med. Biol. Eng. Comput.* **2014**, DOI: 10.1007/s11517–014–1182–6.
[23] H. Hong, Y. Zhang, J. W. Engle, T. R. Nayak, C. P. Theuer, R. J. Nickles, T. E. Barnhart, W. Cai, *Biomaterials* **2012**, *33*, 4147.
[24] A. Cousins, S. K. Thompson, A. B. Wedding, B. Thierry, *Biotechnol. Adv.* **2014**, *32*, 269.
[25] a) Y. Sun, J. Peng, W. Feng, F. Li, *Theranostics* **2013**, *3*, 346; b) X. Huang, F. Zhang, S. Lee, M. Swierczewska, D. O. Kiesewetter, L. Lang, G. Zhang, L. Zhu, H. Gao, H. S. Choi, G. Niu, X. Chen, *Biomaterials* **2012**, *33*, 4370; c) J. Zhou, X. Zhu, M. Chen, Y. Sun, F. Li, *Biomaterials* **2012**, *33*, 6201; d) H. G. van der Poel, T. Buckle, O. R. Brouwer, R. A. Valdés Olmos, F. W. B. van Leeuwen, *Eur. Urol.* **2011**, *60*, 826.

Adv. Mater. **2015**,
DOI: 10.1002/adma.201404739